Magnetic anisotropy of epitaxially grown Co and its alloy thin films

2009 J. Phys.: Condens. Matter 21 185008

(http://iopscience.iop.org/0953-8984/21/18/185008)

J. Phys.: Condens. Matter **21** (2009) 185008 (6pp) doi:10.1088/0953-8984/21/18/185008

Magnetic anisotropy of epitaxially grown Co and its alloy thin films

J-J Wang[1,3], T Sakurai[2], K Oikawa[3], K Ishida[3], N Kikuchi[2], S Okamoto[2], H Sato[2,4], T Shimatsu[4] and O Kitakami[2,5]

[1] Key Laboratory for Anisotropy and Texture of Materials, Northeastern University, Shenyang 110004, People's Republic of China
[2] Institute of Multidisciplinary Research for Advanced Materials, Tohoku University, 2-2-1 Katahira, Sendai 980-8577, Japan
[3] Department of Materials Science, Graduate School of Engineering, Tohoku University, 6-6-02 Aobayama, Sendai 980-8579, Japan
[4] Research Institute of Electrical Communication, Tohoku University, 2-2-1 Katahira, Sendai 980-8577, Japan

E-mail: kitakami@tagen.tohoku.ac.jp

Received 6 August 2008, in final form 8 January 2009
Published 11 March 2009
Online at stacks.iop.org/JPhysCM/21/185008

Abstract
We have performed a systematic study on the correlation between magnetic anisotropy energy (MAE) and crystal structures, such as lattice parameters, stacking fault densities, lattice strain, and so on, for epitaxially grown Co, Co–Pt, and Co–Pd alloy thin films, and have found that the MAE strongly depends on the axial ratio c/a of the hcp crystal lattice. As the c/a of hcp Co decreases down to ∼1.61 which is smaller than 1.622 for bulk Co, the MAE becomes significantly enhanced up to $\sim 10^6$ J m^{-3}. Similar trends have also been verified for hcp Co–Pt and –Pd. These results, which are qualitatively consistent with the classic single-ion anisotropy model and the recent first principles calculation, suggest a new effective way to control the MAE of magnetic thin films.

1. Introduction

Rapid advances in the data density of magnetic recording require large magnetic anisotropy energy (MAE) for recording media to assure long-term data storage. For this purpose, various magnetic materials with large MAE, such as $L1_0$ FePt and Co/Pd, Pt multilayers, have been intensively examined as prospective candidates for future ultra-high density recording. Recently Shimatsu *et al* found giant perpendicular MAE exceeding 10^6 J m^{-3} in disordered Co–Pt alloy films deposited at ambient temperature [1], being much larger than the MAE of bulk Co–Pt alloy [2], evaporated Co–Pt films [3, 4], and Co–Pt $(10\bar{1}0)$ single crystal films [5]. Their detailed study revealed that the MAE greatly depends on the crystal axis ratio c/a of the hcp lattice and is enhanced up to 2×10^6 J m^{-3} as the ratio c/a reduces down to 1.600 which is smaller than the value of 1.622 for bulk hexagonal-closed-packed (hcp) Co [6, 7]. Such dependence of the MAE on the ratio c/a is in qualitative accord with both the classic single-ion anisotropy model [1, 8, 9] and the recent first principles calculation [7]. On the other hand, numerous experiments on Co–Pt binary alloy films have verified the strong perpendicular MAE stemming from long- or short-range anisotropic chemical ordering [10] caused by oscillatory surface segregation during thin film growth [11–15]. To elucidate the origin of the giant MAE mentioned above, more extended and elaborate studies are obviously necessary.

In the present study, we investigate the lattice strain effect on the MAE of hcp Co(00·1), (10·0) epitaxial films without any influence of anisotropic chemical ordering commonly found in Co–Pt alloy thin films. Next we report on the MAE of Co–Pt and Co–Pd epitaxial films and discuss the lattice strain and chemical ordering effects on the MAE.

2. Experimental aspects

Co(0001) and Co–Pt(0001), hcp Co–Pd(0001) and fcc Co–Pd(111) thin films were grown on MgO(111) covered with 10 nm thick Ru(0001) underlayers. Co$(10\bar{1}0)$ films were

[5] Author to whom any correspondence should be addressed.

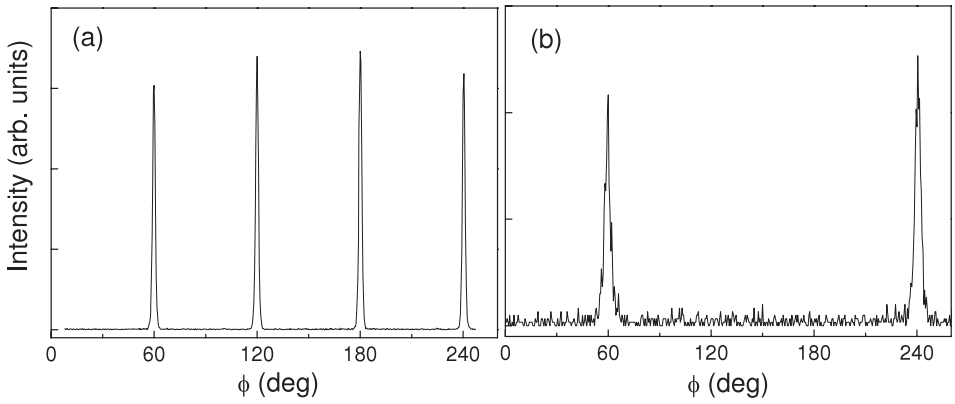

Figure 1. Typical ϕ-scans for $\{10\bar{1}1\}$ planes of (a) Co(0001)/Ru(0001)/MgO(111) and (b) Co$(10\bar{1}0)$/Cr(211)/MgO(110).

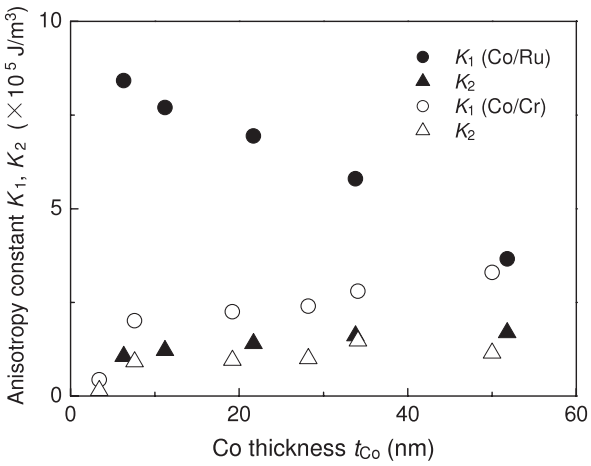

Figure 2. Uniaxial magnetic anisotropy constants K_1 and K_2 of Co(00·1)/Ru and Co(10·0)/Cr as functions of Co thickness t_{Co}.

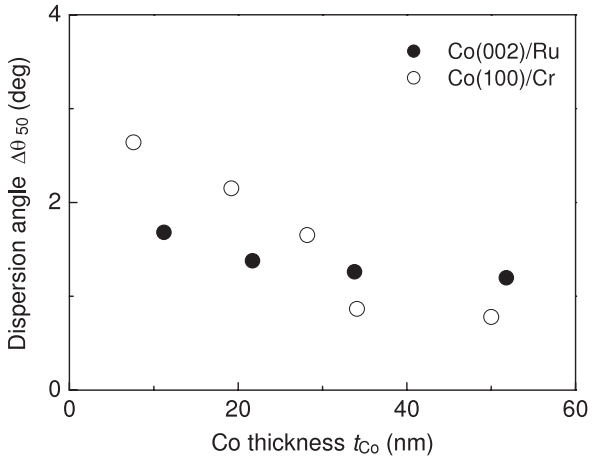

Figure 3. Mosaic spreads of Co(00·1)/Ru and Co(10·0)/Cr evaluated from the full width at half maximum of the rocking curves in the symmetric geometry.

grown on MgO(110) covered with 10 nm thick Cr(211) underlayers. The sputtering chamber was evacuated down to 1×10^{-6} Pa prior to film depositions. The growth temperature and Ar gas pressure were optimized to 573 K and 0.65 Pa, respectively. The film compositions were confirmed by the energy-dispersive x-ray spectroscopy. The magnetization loops were obtained by the anomalous Hall effect (AHE) along with vibrating sample magnetometry. The uniaxial magnetic anisotropy energy is given by $\varepsilon_K = K_1 \sin^2\theta + K_2 \sin^4\theta = -\frac{1}{2}K_u \cos 2\theta + \frac{1}{8}K_2 \cos 4\theta +$ constant, where the twofold symmetry component of the MAE is given as $K_u = K_1 + K_2$ and the angle θ denotes the magnetization direction with respect to the easy axis. The magnetic anisotropy constants were determined by subtracting the shape anisotropy from the values measured by the conventional out-of-plane torque magnetometry. For comparison, the anisotropy constants were also evaluated by the generalized Sucksmith–Thompson method [16]. It was found that the values determined by the above two methods agreed very well [17]. The crystal structures were examined by the x-ray diffraction (XRD) with Cu Kα radiation. For each sample, XRD measurements were done to determine the lattice parameters, the film structure, the mosaic spread, the epitaxial relationship, the stacking fault densities, and the volume fraction of fcc regions in the films. Typical examples of the ϕ-scans for $\{10\bar{1}1\}$ planes of (a) Co(0001)/Ru(0001)/MgO(111) and (b) Co$(10\bar{1}0)$/Cr(211)/MgO(110) are illustrated in figure 1. From these ϕ-scans, the epitaxial relationship of our samples was determined as

Co$(0001)[10\bar{1}0]$ ∥ Ru$(0001)[10\bar{1}0]$ ∥ MgO$(111)[110]$
for hcp Co, Co–Pt, Pd

Co$(10\bar{1}0)[0001]$ ∥ Cr$(211)[01\bar{1}]$ ∥ MgO$(110)[001]$
for hcp Co, Co–Pt, Pd

Co$(111)[110]$ ∥ Ru$(0001)[10\bar{1}0]$ ∥ MgO$(111)[110]$
for fcc Co–Pd.

The probabilities of finding deformation and growth stacking faults denoted by α and β were determined from the widths of the $(10\bar{1}2)$ and $(10\bar{1}3)$ diffraction peaks after accounting for grain size [18, 19]. These peaks were measured after tilting the scattering vector with respect to the film normal such that the scans went through the maximum in those peaks. The fcc concentration in the hcp Co and Co–Pt, –Pd films was quantified from the integrated intensities of the hcp$(10\bar{1}1)$ and fcc(111) peaks, taking into account the multiplicity, form

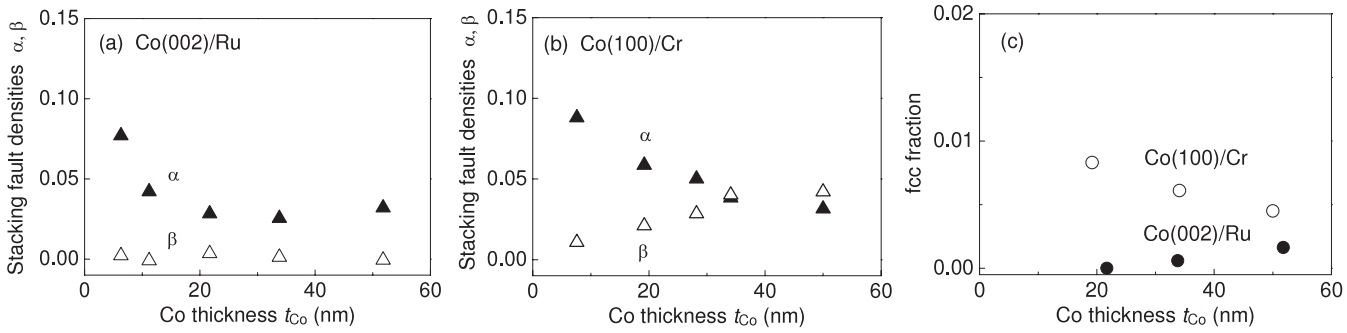

Figure 4. Deformation and growth stacking fault densities, α and β for (a) Co(00·1)/Ru and (b) Co(10·0)/Cr as functions of Co thickness. (c) shows the fraction of fcc Co in the hcp matrix.

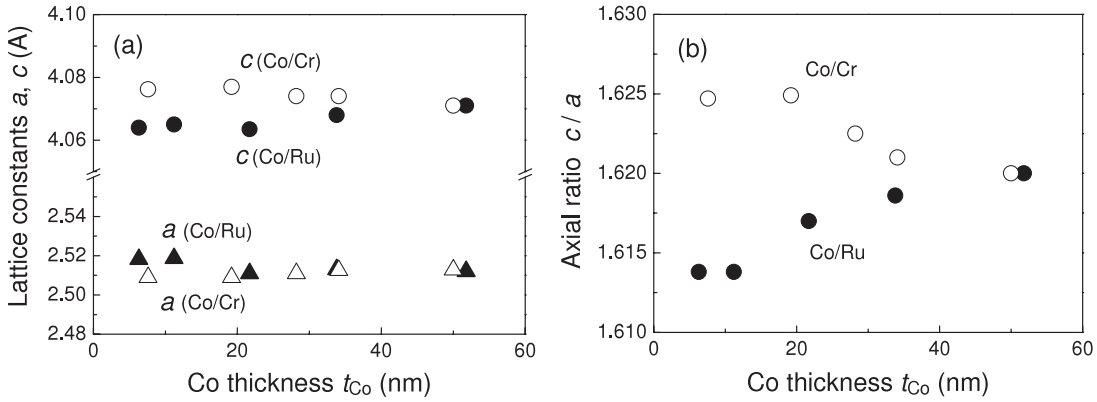

Figure 5. (a) Lattice constants a, c, and (b) axial ratio c/a as functions of Co thickness for Co(00·1)/Ru and Co(10·0)/Cr.

factor, Lorentz polarization factor, and Debye–Waller factor. The accuracy of lattice constant determination by XRD can be improved appreciably by adoption of the Cohen's method [20] using the Nelson–Riley function [21], as described in detail elsewhere [22].

3. Results and discussion

Figure 2 shows the uniaxial magnetic anisotropy constants K_1 and K_2 of Co(00·1)/Ru and Co(10·0)/Cr as functions of Co thickness t_{Co}. As the thickness t_{Co} increases, the MAE of Co/Cr gradually increases and approaches the values of bulk hcp Co ($K_1 = 4.5 \times 10^5$ J m^{-3}, $K_2 = 1.5 \times 10^5$ J m^{-3}) [23]. In contrast, the MAE of Co/Ru exceeds 8×10^5 J m^{-3} at $t_{Co} = 5$ nm and subsequently decreases toward the bulk values with the increase in t_{Co}. Such large perpendicular MAE of very thin Co/Ru films is comparable to the giant MAE found in Co–Pt, Co–Pt-Cr/Ru films [1, 6, 7]. This result shows that the large MAE can be induced even in the absence of the anisotropic chemical ordering frequently observed in Co–Pt [10]. To elucidate the origin of the huge MAE of Co, we performed detailed structural studies, as will be mentioned below.

The mosaic spreads of Co(00·1)/Ru and Co(10·0)/Cr were evaluated from the full width at half maximum $\Delta\theta_{50}$ of the rocking curves (ω scans) in the symmetric geometry. As shown in figure 3, the spread angle $\Delta\theta_{50}$ is less than 2.5° for both Co(00·1) and Co(10·0) over the Co thickness range

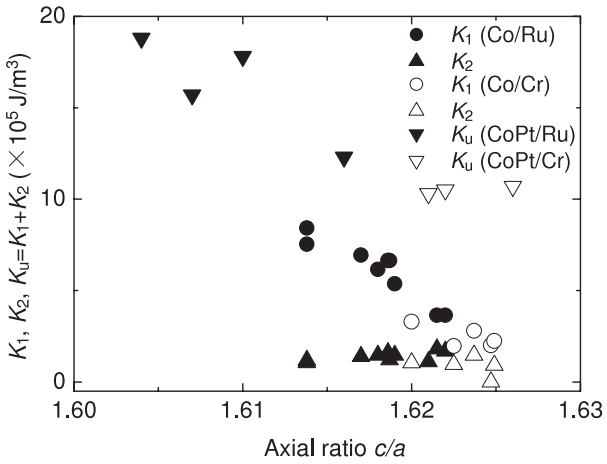

Figure 6. Magnetic anisotropy constants versus axial ratio c/a for Co/Ru, Cr and $Co_{80}Pt_{20}$/Ru, Cr. For $Co_{80}Pt_{20}$, the twofold symmetry components K_u of the MAE are shown.

examined in the present study. Figures 4(a) and (b) shows the deformation and growth stacking fault densities, α and β, for Co(00·1) and Co(10·0), respectively. Both α and β are quite small and no distinct difference is found between Co(00·1) and Co(10·0), except for higher stacking fault densities for the latter. Figure 4(c) shows the fraction of fcc Co in the hcp matrix. We note that the fcc fraction is negligibly small for both Co(00·1) and Co(10·0) while the latter exhibits

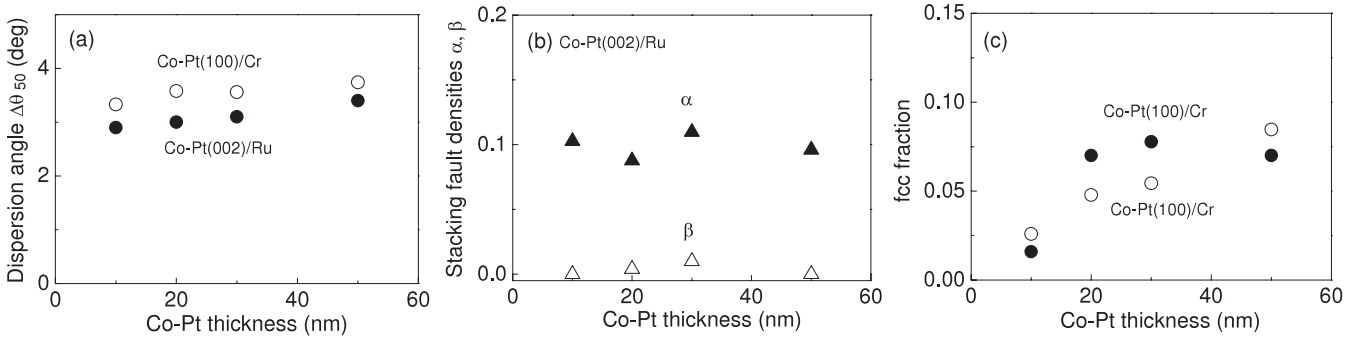

Figure 7. (a) Mosaic spread $\Delta\theta_{50}$, (b) stacking fault densities α and β, and (c) fcc fraction as functions of Co–Pt thickness for $Co_{80}Pt_{20}(0001)$/Ru(0001)/MgO(111) and $Co_{80}Pt_{20}(10\bar{1}0)$/Cr(211)/MgO(110).

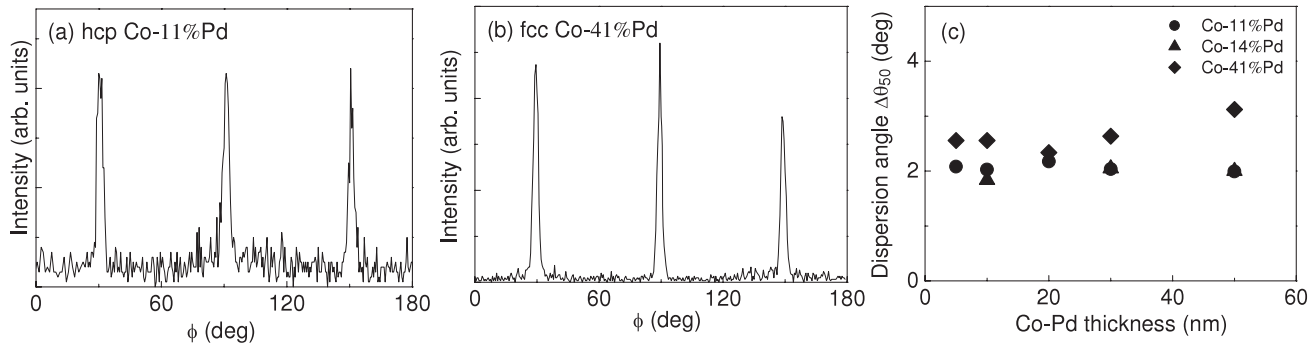

Figure 8. Typical ϕ-scans for (a) $\{10\bar{1}1\}$ of hcp $Co_{89}Pd_{11}(10{\cdot}1)$ and (b) {111} of fcc $Co_{59}Pd_{41}(111)$, and (c) mosaic spreads $\Delta\theta_{50}$ of hcp Co–Pd(0001) and fcc (111).

somewhat larger fcc fraction. The lattice constants a, c and the axial ratio c/a are shown in figure 5. As the thickness t_{Co} of Co(10·0)/Cr increases, the parameter a increases and c decreases very gradually, resulting in the decrease in the axial ratio c/a with t_{Co}. On the other hand, for Co(00·1)/Ru, a increases and c decreases with decreasing t_{Co}, resulting in an appreciable decrease of c/a with decreasing t_{Co}. Comparing the variation of c/a in figure 5 and the MAE in figure 2, there seems to exist a correlation between the K_1 and the axial ratio c/a. Figure 6 clearly demonstrates the strong correlation of the magnetic anisotropy K_1 with the axial ratio c/a, that is, the K_1 is significantly enhanced with the reduction of the axial ratio c/a. This result is qualitatively consistent with the predictions based on the classic single-ion anisotropy model [1, 8, 9] and the first principles calculation [7]. Based on the simple ligand field concept [24–26], the MAE is proportional to the spin–orbit coupling strength and the anisotropy of the orbital moment $(m_0^{\perp} - m_0^{\parallel})$, where $m_0^{\perp}$ and $m_0^{\parallel}$ represent the orbital moments for the case when the sample is magnetized out-of-plane and in-plane, respectively. According to the first principles calculation on hcp Co by Sakuma and Tanii [27], the anisotropy of the orbital moment $(m_0^{\perp} - m_0^{\parallel})$ increases with decreasing the axial ratio c/a, resulting in a larger perpendicular MAE. We also performed similar studies on $Co_{80}Pt_{20}(0001)$/Ru(0001)/MgO(111) and $Co_{80}Pt_{20}(10{\cdot}0)$/Cr(211)/MgO(110). The structural parameters, the mosaic spread $\Delta\theta_{50}$, stacking fault densities α and β, and the fcc fraction, are shown in figure 7. Note that slightly deteriorated but good crystal quality of the hcp structure is again maintained in spite of somewhat large Pt concentration. No indication of the long-range chemical ordering, such as $L1_2$-, DO_{19}-, and DO'_{19}-type ordered compounds [28], was verified by XRD and electron diffraction. Figure 6 plots the K_u of CoPt(00·1)/Ru and CoPt(10·0)/Cr against the axial ratio. A very similar c/a dependence as for pure Co is confirmed, except that CoPt exhibits an MAE twice as large as that for Co.

As mentioned above, the MAE of hcp Co and its alloy films is considerably influenced by the lattice strain and can be enhanced to $\sim 10^6$ J m^{-3} which is comparable to the MAE of some ordered alloys, such as $L1_0$ FePt etc, even in the absence of the obvious long-range anisotropic chemical ordering found in evaporated Co–Pt films [10, 29, 30]. Our next concern is how the MAE varies when the crystal structure changes from the hcp structure to the fcc one. For this study, we selected a Co–Pd binary system because it forms a continuous solid solution and its equilibrium phase changes from the hcp to the fcc at a Pd concentration of around 20 at.% [31]. In accordance with the phase diagram, the crystal structure of $Co_{100-x}Pd_x(0001)$ films grown on Ru/MgO(111) changed from hcp to fcc at around $x \sim 20$ at.%. Figures 8(a) and (b), respectively, show the typical ϕ-scans for hcp $Co_{89}Pd_{11}(10{\cdot}1)$ and fcc $Co_{59}Pd_{41}(111)$, and the mosaic spread $\Delta\theta_{50}$ of hcp Co–Pd(0002) and fcc (111) are plotted in figure 8(c). Note that good epitaxial growth on Ru/MgO(111) is realized all over the Pd concentration and the thickness examined in the present study. Figure 9(a) shows the fraction of fcc phase.

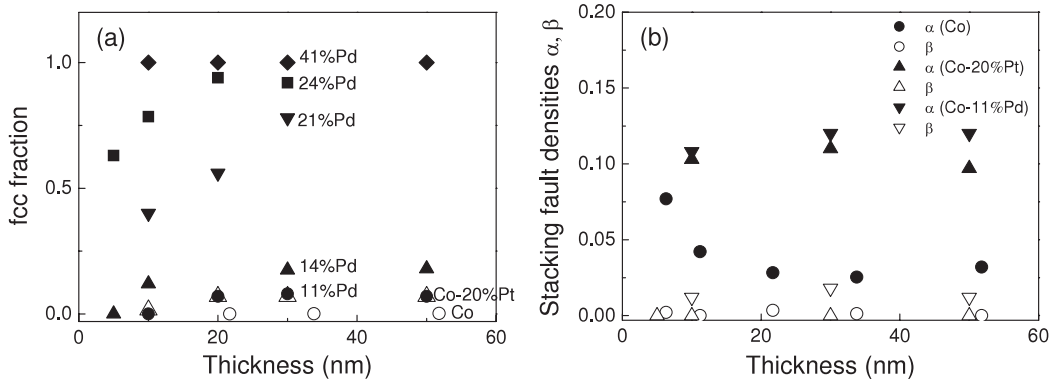

Figure 9. (a) Fcc fraction and (b) deformation and growth stacking fault densities, α and β, of Co–Pd films as functions of Co–Pd thickness. In (a), for comparison, the data of Co and $Co_{80}Pt_{20}$ are also plotted as empty symbols.

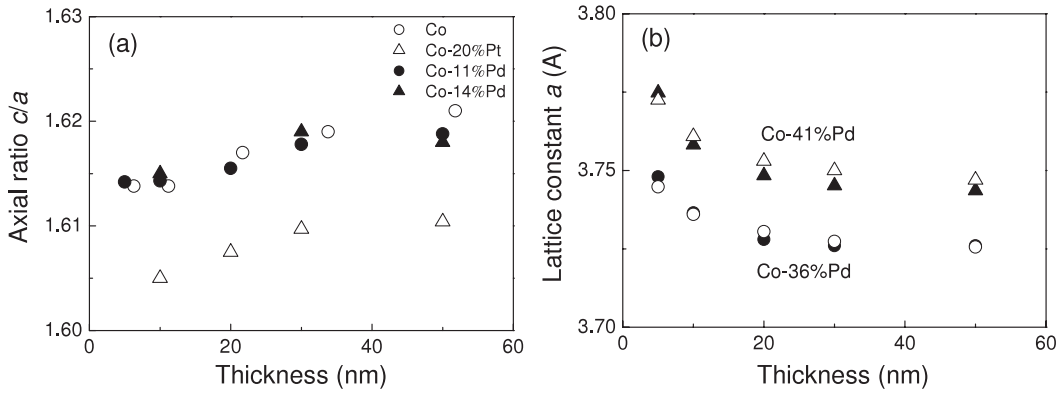

Figure 10. (a) Axial ratio c/a of hcp Co–Pd and (b) lattice parameters a of the fcc Co–Pd determined from the two different diffractions; one is from the fcc(111) parallel to the film plane, the other is from the fcc(200) which makes an angle of 76° with the film plane. In (a), the data of Co and $Co_{80}Pt_{20}$ are also plotted as empty symbols for comparison.

The fcc fraction is small for $x < 20$, coexists with the hcp phase at $x \sim 20$, and becomes dominant for $x > 25$. The stacking fault densities of the $Co_{89}Pd_{11}$ film are comparable to those of Co and $Co_{82}Pt_{20}$, as shown in figure 9(b). The lattice parameters of hcp- and fcc-Co–Pd are shown in figures 10(a) and (b), respectively. The lattice parameters a of the fcc phase were determined from the two different diffractions; one is from the fcc(111) parallel to the film plane, the other is from the fcc(200) which makes an angle of 76° with the film plane. The axial ratio c/a decreases with decreasing the Co–Pd thickness as in the hcp Co and Co–Pt films also plotted in figure 10(a) for comparison. On the other hand, no obvious anisotropic deformation is observed in the fcc Co–Pd films since the two lattice parameters a evaluated from fcc(111) and (200) diffraction peaks coincide well with each other. We note that the fcc lattice isotropically expands with decreasing the film thickness, probably due to the lattice misfit between Co–Pd and Ru although the details are unknown.

The perpendicular magnetic anisotropy K_u of hcp Co–Pd(00·1) and fcc Co–Pd(111) is plotted against the film thickness in figure 11. For hcp Co–Pd, there again exists a correlation between the K_u and the axial ratio c/a in figure 10(a) similarly to hcp Co and Co–Pt in figure 6. It is interesting to note that the fcc $Co_{100-x}Pd_x$ ($x > 20$) has a very large K_u of 2×10^5 J m^{-3} in spite of its cubic crystal

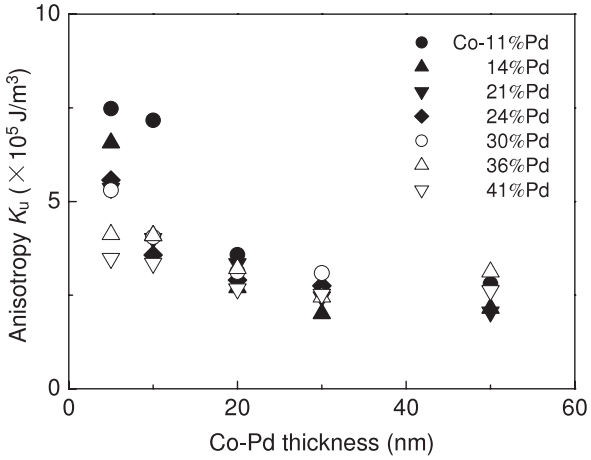

Figure 11. Perpendicular magnetic anisotropy K_u versus Co–Pd thickness for hcp Co–Pd(00·1)/Ru and fcc Co–Pd(111)/Ru.

symmetry. The typical magnetization curves for the 5 nm thick $Co_{59}Pd_{41}$ film are shown in figure 12. Similar results have been reported by Weller *et al* [4]. From the perpendicular anisotropy K_u and the Kerr spectra, they speculate that the large MAE of Co–Pd would be attributable to unidentified growth induced

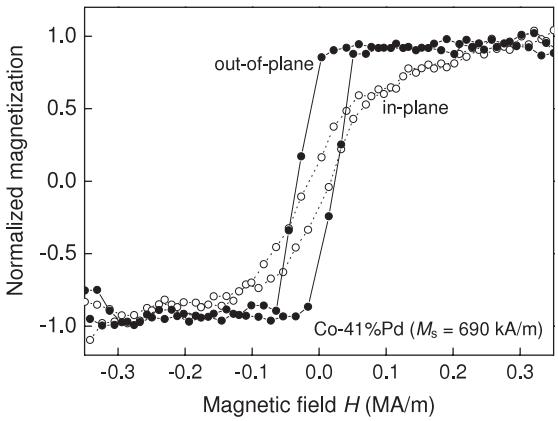

Figure 12. Typical in-plane and out-of-plane magnetization curves for the 5 nm thick fcc $Co_{59}Pd_{41}$(111)/Ru(002)/MgO(111).

heterogeneities, similar to short-range anisotropic chemical ordering in Co–Pt thin films caused by oscillatory surface segregation during thin film growth [10–15]. In spite of no clear evidence for anisotropic chemical ordering, we cannot help accepting that the large MAE of fcc Co–Pd originates from such unidentified anisotropic chemical ordering.

4. Summary

In summary, we have studied the relationship between the magnetic anisotropy energy (MAE) and the crystal structures for Co and its alloys with Pt and Pd. The MAE is found to be closely correlated with the axial ratio c/a of the hcp lattice, that is, the MAE of hcp Co is significantly enhanced up to $\sim 10^6$ J m^{-3} with the reduction of c/a. A very similar trend has also been verified for hcp Co–Pt and -Pd alloys. These results are qualitatively consistent with the predictions based on the classic single-ion anisotropy model and the recent first principles calculation. Another interesting finding is the somewhat large MAE exceeding 10^5 J m^{-3} of fcc Co–Pd films. Although its origin still remains unknown, one possible explanation is the existence of unidentified anisotropic chemical ordering with an extremely short coherence length which is hard to be detected by conventional x-ray and electron diffractions.

Acknowledgments

This work was partly supported by the Core Research for Evolution Science and Technology (CREST), Japan Science and Technology Agency (JST), 'Research and Development for Next-Generation Information Technology of MEXT', Grant-in-Aid for Scientific Research from MEXT, Special Education and Research Expenses from Post-Silicon Materials and Devices Research Alliance, and the Storage Research Consortium in Japan.

References

[1] Shimatsu T *et al* 2004 *IEEE Trans. Magn.* **40** 2483
Shimatsu T *et al* 2005 *IEEE Trans. Magn.* **41** 566
[2] Bolzoni F, Leccabue F, Panizzieri R and Pareti L 1984 *IEEE Trans. Magn.* **20** 1625
[3] Lin C-J and Gorman G L 1992 *Appl. Phys. Lett.* **61** 1600
[4] Weller D, Brändle H, Gorman G, Lin C-J and Nortarys H 1992 *Appl. Phys. Lett.* **61** 2726
Weller D, Brändle H and Chappert C 1993 *J. Magn. Magn. Mater.* **121** 461
[5] Kikuchi N, Kitakami O, Okamoto S, Shimada Y, Sakuma A, Otani Y and Fukamichi K 1999 *J. Phys.: Condens. Matter* **11** L485
[6] Shimatsu T *et al* 2006 *J. Appl. Phys.* **99** 08G908
Shimatsu T *et al* 2007 *IEEE Trans. Magn.* **43** 2995
[7] Shimatsu T, Okazaki Y, Sato H, Muraoka H, Aoi H, Sakurai T, Okamoto S, Kitakami O, Tanii S and Sakuma A 2008 *J. Appl. Phys.* **103** 07F524
[8] Carr W J 1957 *Phys. Rev.* **108** 1158
Carr W J 1958 *Phys. Rev.* **109** 1971
[9] Ono F 1981 *J. Phys. Soc. Japan* **50** 2564
[10] Maret M *et al* 1996 *Thin Solid Films* **275** 224
Maret M *et al* 1997 *J. Magn. Magn. Mater.* **166** 45
Maret M *et al* 1998 *Thin Solid Films* **319** 191
Maret M *et al* 1999 *Eur. Phys. J.* B **7** 347
[11] Gauthier Y, Baudoing-Savois B, Bugnard J M, Bardi U and Atrei A 1992 *Surf. Sci.* **276** 1
[12] Treglia G and Legrand B 1987 *Phys. Rev.* B **35** 4338
[13] Lundberg M 1987 *Phys. Rev.* B **36** 4692
[14] Legrand B, Treglia G and Ducastelle F 1990 *Phys. Rev.* B **41** 4422
[15] Heinrichs S, Dieterich W and Maass P 2007 *Phys. Rev.* B **75** 085437
[16] Okamoto S, Kikuchi N, Kitakami O, Miyazaki T and Shimada Y 2002 *Phys. Rev.* B **66** 024413
Okamoto S, Nishiyama K, Kitakam O and Shimada Y 2001 *J. Appl. Phys.* **90** 4085
[17] Shimatsu T, Sato H, Okazaki Y, Aoi H, Muraoka H, Nakamura Y, Okamoto S and Kitakami O 2006 *J. Appl. Phys.* **99** 08G908
[18] Warren B E 1990 *X-Ray Diffraction* (New York: Dover)
[19] Toney M F, Marinero E E, Doerner M F and Rice P M 2003 *J. Appl. Phys.* **94** 4018
[20] Cohen M U 1935 *Rev. Sci. Instrum.* **6** 68
Cohen M U 1936 *Rev. Sci. Instrum.* **7** 155
[21] Culity D B 1978 *Elements of X-Ray Diffraction* (London: Addison-Wesley)
[22] Okamoto S, Kitakami O and Shimada Y 2000 *J. Magn. Magn. Mater.* **208** 102
[23] Chikazumi S 1997 *Physics of Ferromagnetism* (Oxford: Clarendon)
[24] Bruno P 1989 *Phys. Rev.* B **39** 865
[25] Wang D, Wu R and Freeman A J 1993 *Phys. Rev.* B **47** 14932
[26] Stohr J 1999 *J. Magn. Magn. Mater.* **200** 470
[27] Tanii S and Sakuma A 2007 private communication
Tanii S 2007 *Master of Engineering Thesis* Tohoku University
[28] Moraitis G, Parlebas J C and Khan M A 1996 *J. Phys.: Condens. Matter* **8** 1151
[29] Harp G R, Weller D, Rabedeau T A, Farrow R F C and Toney M F 1993 *Phys. Rev. Lett.* **71** 2493
[30] Maret M, Cadevnie M C, Herr A, Poinsot R, Beaurepaire E, Lefebvre S and Bessière M 1999 *J. Magn. Magn. Mater.* **191** 61
[31] Hansen M and Anderko K 1958 *Constitution of Binary Alloys* (New York: McGraw-Hill)